

Stochastic approach to the design of a simple structure under the risk of liquefaction

P.S. Koutsourelakis, J.H. Prevost & G. Deodatis
Department of Civil and Environmental Engineering, Princeton University

ABSTRACT: The present study deals with the nonlinear stochastic dynamic analysis of a soil-structure interacting system. The ultimate objective is to determine the risk of damage to the system due to liquefaction under a wide range of earthquake intensities. A Monte Carlo simulation approach is followed in conjunction with advanced finite element procedures. The stochastic spatial variability of soil properties and the randomness of the seismic excitation are taken into account in order to estimate the statistics of the response. Specifically, soil properties are modeled as non-Gaussian random fields and seismic excitations as nonstationary random processes. The probabilistic characteristics of the stochastic field modeling soil properties are established from in-situ tests. The risk of damage to the soil-structure system due to liquefaction is assessed by establishing fragility curves, which are of paramount importance for risk assessment and management studies of such systems. The relative effect of the variability of various soil parameters on the variability of the response is also examined.

1 INTRODUCTION

One of the most difficult phenomena to account for in geotechnical design is the interaction between the structure and the soil. The properties of the latter can vary tremendously, exhibit strong inhomogeneity and are in general difficult to measure or estimate. A rational and realistic approach therefore has to consider these uncertainties and formulate failure criteria in a probabilistic setting. Furthermore, in dynamical problems another component of uncertainty is the earthquake itself. It exhibits variability in terms of intensity, duration and frequency content, which have to be taken into consideration as well.

The scope of this study is to incorporate the stochasticity induced by these factors, to measure their effect on the behavior of a soil-structure system and to assess the risks in geotechnical design. In particular, a dynamic analysis of a simple structure based on a rigid foundation and located on top of a saturated sand layer, is performed (see Figure 1). For design purposes, the results are condensed and presented in the form of fragility curves. The latter depict the probability of exceeding various thresholds in the response, each corresponding to a different level of damage, with respect to the earthquake intensity. In order to integrate the multiple sources of uncertainty and the intricate non-linear behavior of the system, Monte-Carlo simulations are carried out.

The first few sections are devoted to the explanation of the model adopted to describe the uncertainties of the soil and the earthquake motion. They are followed by a presentation of the results of the analysis and the conclusions that are drawn. Finally, a sensitivity analysis is performed in order to determine the relative effect of different parameters that come into the design.

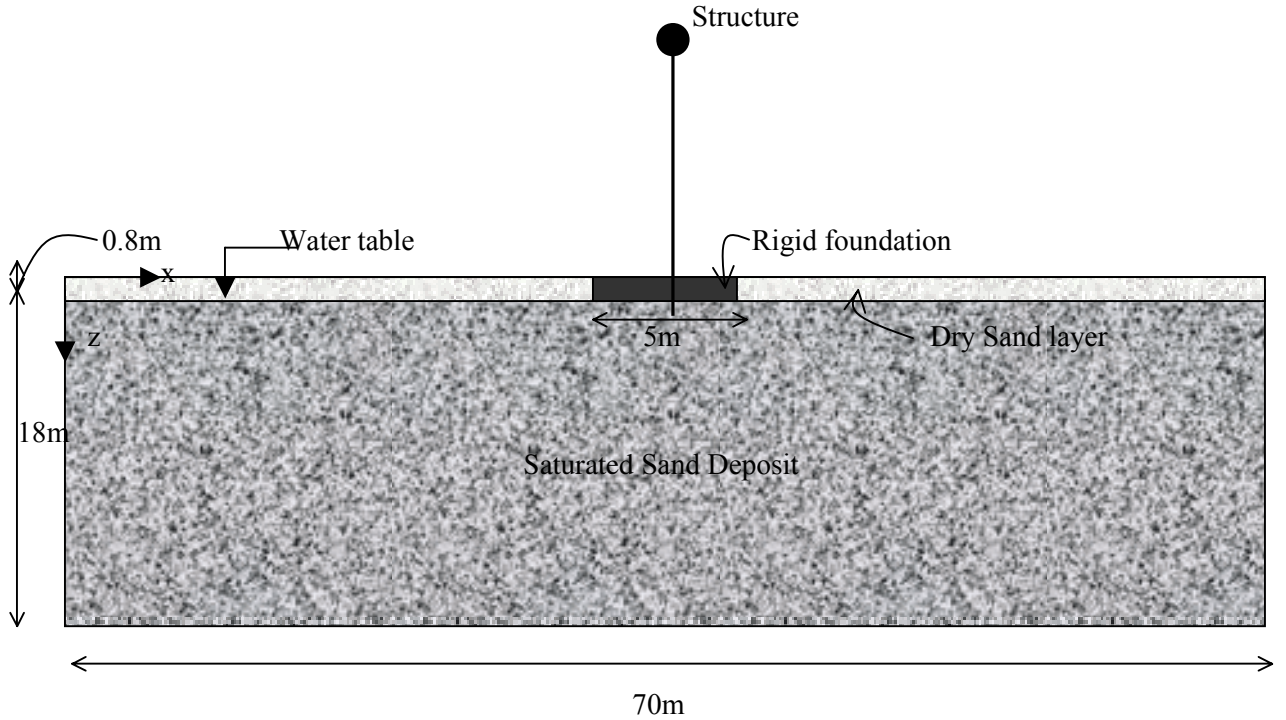


Figure 1. Problem Configuration.

2 SOIL PROPERTIES

It is well known from practice and experiments that excess pore pressures can develop inside a saturated sand deposit. They play an important role in the overall behavior of the system and can ultimately lead to failure due to liquefaction during a seismic event. In order to account for the latter, the soil is modeled as a two-phase material (saturated porous solid-water system) and two coupled sets of differential equations are solved simultaneously (see Prévost, 1980).

An elaborate multi yield-surface plasticity model (Prévost, 1985) describes the constitutive behavior of the solid phase. In particular, it is a kinematical hardening model, defined by a collection of nested *Drucker-Prager* type yield surfaces. The yield surfaces define regions of constant shear moduli and in this manner the model discretizes the smooth elastic-plastic stress-strain curve into N linear segments ($N=20$ in this study).

The plastic flow rule is associative in its deviatoric component and non-associative in its dilatational component.

The constitutive parameters of the model can be categorized as follows:

State parameters, which include the solid mass density ρ_s , the porosity n and the permeability \mathbf{k} (isotropic).

Low strain moduli parameters such as the shear G_0 and bulk B_0 moduli. A dependence of these moduli on the effective mean normal stress p' is assumed, which introduces two more parameters.

Yield surface and failure parameters, which are related with the kinematic hardening rule, the size of the surfaces and the plastic modulus. They include the friction angle at failure φ , maximum deviatoric strain ϵ_{dev}^{max} , a stress-strain curve coefficient α and the low strain shear modulus G_0 . One more parameter, the coefficient of lateral stresses k_0 , is needed to evaluate the initial position of the yield surfaces. It was set equal to 0.54 in this study.

Finally, *dilation parameters* that are used to evaluate the dilatational part of the plastic potential.

They are the dilation angle $\bar{\varphi}$ and the parameter X_{pp} used in the definition of the flow rule for the dilatational component.

2.1 Evaluation of probabilistic characteristics of soil properties

The establishment of probabilistic models for the soil properties was based on in-situ CPT tests that have been performed in a location called Tarsiut P-45 (Jefferies et al., 1985, 1988) on an artificial island constructed in the Canadian Beaufort Shelf. The estimation of other soil properties necessary for the analysis was done from the CPT values using a series of empirical relations (Popescu 1995). The CPT data collected from several borings of these in-situ measurements (Gulf Canada Res. Inc. 1984) were subjected to field data transformation, extraction of first order probability structure and finally extraction of correlation structure (Popescu et al. 1997).

The first procedure consisted of the cumbersome task of filtering and smoothing the raw data. A (statistically) homogeneous set of CPT values was obtained by subtracting the spatial trend $CPT^{av}(z)$ and dividing by the sample standard deviation $CPT^{std}(z)$. This standardization is depicted in the following equation:

$$CPT^r(z) = \frac{CPT(z) - CPT^{av}(z)}{CPT^{std}(z)} \quad (1)$$

where $CPT(z)$ is the original sample (before standardization). Subsequently, a theoretical model was fitted to the empirical probability distribution of the standardized data. It was found that a beta distribution, defined in the interval $[-2.05, 10.97]$ provided the best fit. This distribution has a skewness of 0.76 and kurtosis 3.58. As for the correlation structure of the CPT data, a separable model for the autocorrelation function of the form:

$$R(\Delta x, \Delta z) = R_x(\Delta x)R_z(\Delta z) \quad (2)$$

seemed most appropriate in this case. It is worth mentioning that the correlation distance is $\theta_z = 0.95m$ in the z direction (depth) and $\theta_x = 12.1m$ in the x (horizontal) direction (Fig. 2). These values indicate significantly more variability in depth rather than horizontally. Stochastic field models to represent the spatial variability of soil properties have been used also by Fenton (1999) and Griffiths & Fenton (2000).

2.2 Generation of sample functions of soil properties

As part of the Monte Carlo approach that was followed, sample functions of the non-Gaussian, two-dimensional homogeneous stochastic field $CPT(x, z)$, modeling the CPT values, were generated.

Due to the major computational effort necessary to solve the deterministic nonlinear dynamic problem involved in this study, it was decided to use fifty samples in the Monte Carlo simulation procedure. A methodology based on the theory of translation processes (Grigoriu 1995) involving the mapping from a Gaussian to a non-Gaussian process was chosen.

The ensemble autocorrelation function of fifty non-Gaussian sample functions generated is shown in Figure 3. The corresponding target autocorrelation function is plotted in Fig. 2. It is easily observed that the ensemble autocorrelation function is reasonably close to the corresponding target.

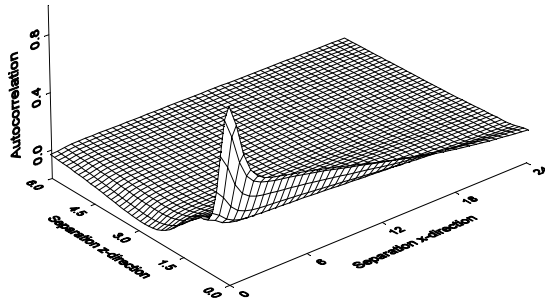


Figure 2. Target autocorrelation function for CPT values.

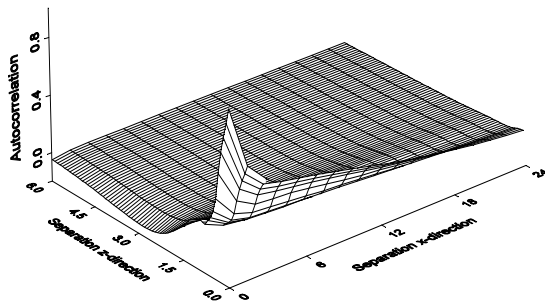


Figure 3. Ensemble autocorrelation computed from 50 sample functions generated.

3 GENERATION OF SEISMIC GROUND MOTION TIME HISTORIES

As mentioned earlier, the earthquake loading is also a significant factor of uncertainty in the problem. It exhibits randomness in its intensity, frequency content and duration.

A methodology described in detail in Gasparini and Vanmarcke (1976) and Deodatis (1996) was used to generate sample functions of acceleration time histories to be compatible with a target response spectrum and to have a prescribed duration of strong ground motion defined through an envelope function.

For the present study, two different response spectra were selected:

- a) *Spectrum 1*: the 1997 Uniform Building Code's response spectrum corresponding to rock-stiff soils (UBC 1997).
- b) *Spectrum 2*: a fictitious response spectrum rich in low frequencies (high periods) that is believed to be indicative of a near-field event (Popescu et al. 1997).

These two acceleration response spectra (RSA), normalized to the peak ground acceleration (PGA), are plotted in Figure 4. The procedure for the generation of the earthquake acceleration time histories is iterative. In order to account for the variability in the duration of the actual earthquake, two different envelope functions were used, according to the Jennings et al. (1968) model, resulting in durations of 12sec and 20sec.

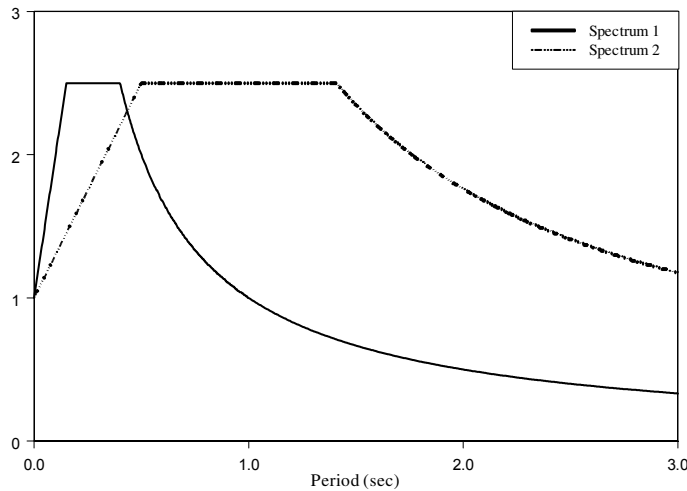


Figure 4. Target acceleration response spectra selected

Finally, in order to account for the variation in the intensity of the earthquake, six different values for the peak ground acceleration were used, namely 0.1g, 0.125g, 0.15g, 0.175g, 0.2g and 0.3g. In sum mary, the number of different possible earthquakes that were considered in this study was:

$$(2 \text{ spectra}) \times (2 \text{ durations}) \times (6 \text{ PGAs}) = 24 \text{ cases}$$

4 FINITE ELEMENT MESH – PROBLEM FORMULATION

The stochastic field that is generated on a regular periodic mesh (modeling soil properties) had to be transferred onto the finite element mesh. In order to do that the midpoint method was adopted, according to which, the random field is represented by its value at the centroid of each element. This method has the advantage of preserving the first order probability and correlation structure in contrast to other techniques such as local averaging that do not.

The upper bounds for the element size depend on the correlation distances θ_x and θ_z . In this study, the maximum element size was 1.5m in the x direction and 0.5m in the z direction (see Popescu 1995).

A rigid block of dimensions $0.8m \times 5.0m$ models the foundation. A single oscillator system on top of the foundation is playing the role of the superstructure (see Fig. 1). It consists of a nodal mass connected to the foundation system by linear beam elements. In order to account for different types of structures, the beam stiffness was varied in order to obtain three different cases with fundamental lateral frequencies of $\omega = 3, 5$ and 10 rad/sec (periods of $T = 2.1, 1.3$ and 0.63 sec , respectively). Finally, a load of 150KPa was considered on top of the footing. This is the maximum allowed design load calculated from a standard deterministic design analysis.

In conclusion, it is worth summarizing the procedure followed to perform the analysis:

- Sample functions of random field $CPT^r(x, z)$ are first generated, and then multiplied by the spatial standard deviation $CPT^{std}(z)$. Eventually, the spatial trend $CPT^{av}(z)$ is added to obtain sample functions of the actual field $CPT(x, z)$, modeling the CPT values.
- Empirical relations are used to compute the values of a number of soil parameters at the centroid of each finite element from the simulated CPT values.

- For each of the soil sample functions obtained in this way, earthquake ground motion time histories are generated for all possible cases of response spectra (2), durations (2) and PGAs (6) (a total of 24 acceleration time histories). These time histories are used as input excitation at the base of the mesh in order to carry out the nonlinear dynamic analysis.
- The response of the system is recorded in terms of the (maximum) uniform foundation settlement and (maximum) foundation tilting. The latter is measured as the differential settlement at the ends of the footing over its length (5m).
- These results are finally used to establish fragility curves and other statistical measures of the response.

The calculations were performed with the finite element code Dynaflow (Prévost, 1999).

5 NUMERICAL RESULTS

Before embarking in the presentation of the results, it is worth devoting some space to discuss the merits of the stochastic approach followed in this study.

5.1 *Deterministic vs. Stochastic approach for description of soil properties*

In terms of the foundation response, Figure 5 plots the time history of the foundation tilt when using average (deterministic) CPT values, and when using three different sample functions of simulated stochastic soil properties.

Comparison of the four curves in this figure indicates that the assumption of average (deterministic) soil properties can underestimate considerably the values of the foundation tilt. This can be explained from the fact that the stochastic representation of soil properties produces weak soil pockets that control to a large extent the magnitude of the response. These weak soil pockets cannot be described when using average (deterministic) soil properties.

In order to isolate the effect of different assumptions for the description of soil properties in Fig. 5, the same input earthquake time history was used to obtain all four curves. Now, in order to study the effect of different ground motion time histories, Fig. 6 plots the time history of the uniform foundation settlement for four different earthquake motions using the same (simulated) soil properties. All four input time histories have the same peak ground acceleration, but their duration and frequency content are different. The first one is an actual record from the 1964 Niigata earthquake, while the other three time histories are simulated records using the procedure described in Section 3.

It becomes immediately obvious that the four curves have significant differences, indicating that the PGA is not the optimum parameter to predict the system's response in the case examined here. In addition, the stochastic approach to model the input ground motion time histories is able to describe the considerable variability in the response that is actually observed in practice.

5.2 *Results of stochastic analysis - Effect of ground motion parameters*

In this section, the results are presented in the form of the maximum value of the response (settlement or tilt) that was observed during the phenomenon.

A problem that arose during this study was that for some combinations of sample functions of soil properties and earthquake time histories, the finite element algorithm was unable to provide a solution. This computational problem was due to the fact that at extended areas within the soil volume, the pore water pressure increased to levels comparable to the effective mean stress and consequently the soil strength dropped to zero. Eventually the algorithm broke down, convergence could not be achieved in the solution and computations stopped. To the authors' best knowledge, there is no currently available finite element algorithm capable of overcoming this problem. In the following, different approaches will be used to portray the results of these cases where the finite element algorithm diverged and computations stopped.

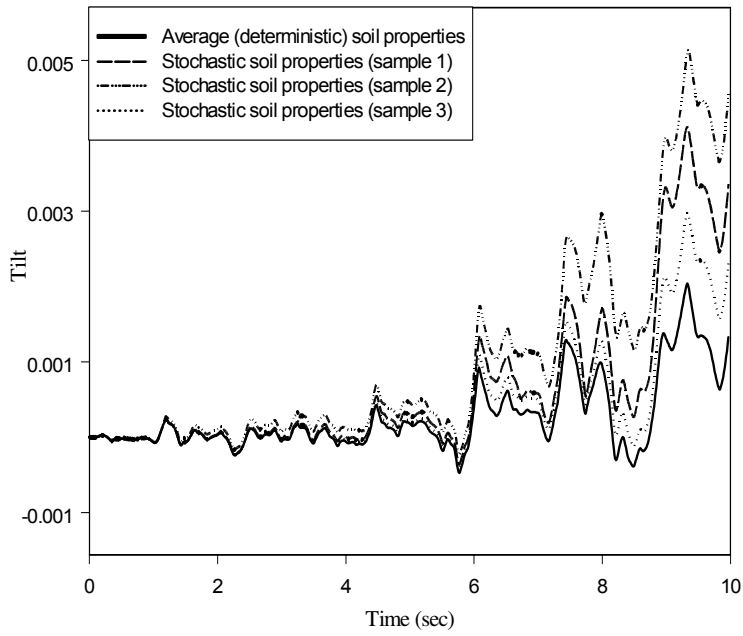


Figure 5. Time history of foundation tilt – Comparison of different assumptions for soil properties

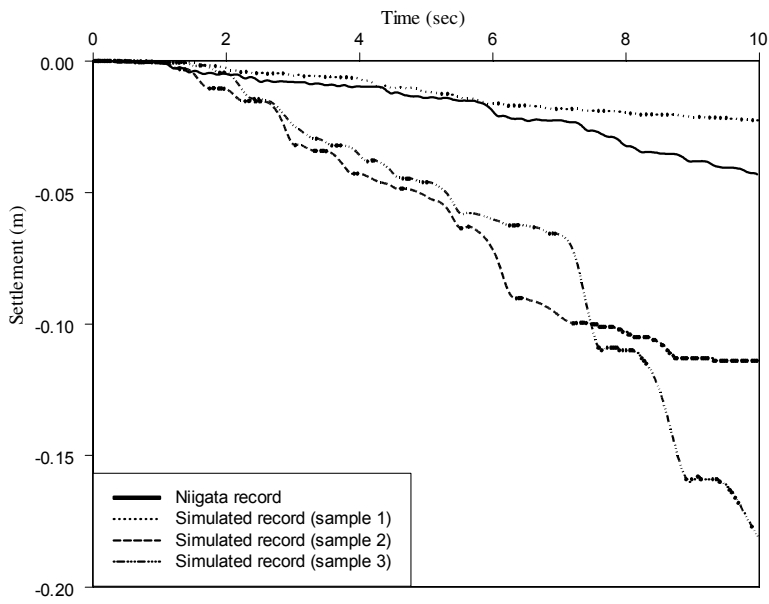


Figure 6. Time history of foundation settlement – Comparison of different earthquakes

An illustrative way to study the results is in the form of scatter plots that provide an insight on the amount of scatter of the peak response values as a function of the severity of the earthquake. Figure 7 displays the scatter plots of the maximum values of the tilt of the foundation for the two response spectra used in this study. On the x-axis of the diagram in Fig. 7, the PGA was used as the measure of the earthquake severity. It is obvious that for the second response spectrum, the maximum foundation response is significantly higher. It should be mentioned that for the cases where the finite element computations were interrupted (which exceeded 50% of the total runs for PGA greater than 0.2g), the maximum value of the response and the PGA up to the time where divergence occurred are plotted in Fig. 7. For the sample runs that exhibited divergence, the maximum value of the response (settlement or tilt) computed before the interruption of calculations is believed to be considerably smaller than the “real” maximum value of the response that would have been obtained if it were possible to continue the calculations. This is the reason that the scatter of the values of the maximum response beyond approximately 0.2g seems to stabilize (or even decrease).

To study the effect of the duration of the earthquake, the scatter plot of Fig. 8 is provided. It should be noted that in contrast with Fig. 7, the cases where the algorithm failed to converge are now omitted. Again, as in Fig. 7, the omitted cases create the illusion of a stabilization or decline of the level of scatter beyond 0.2g. As expected in such a nonlinear dynamic problem with stiffness degradation, earthquakes with longer duration produce larger maximum foundation responses, even though their frequency content (spectrum) and PGA are the same.

It is generally accepted that the PGA is not an ideal measure of the severity/intensity of the earthquake, as it doesn't contain any information about the duration and the frequency content of strong ground motion. Herein, two alternative measures are considered: the root mean square acceleration (I_{rms}) and the Arias intensity (I_{Arias}). The first is defined as:

$$I_{rms} = \sqrt{\frac{1}{T_d} \int_0^{T_d} [a(t)]^2 dt} \quad [\text{m/sec}^2] \quad (3)$$

and the second as:

$$I_{Arias} = \frac{\pi}{2g} \int_0^{T_d} [a(t)]^2 dt \quad [\text{m/sec}] \quad (4)$$

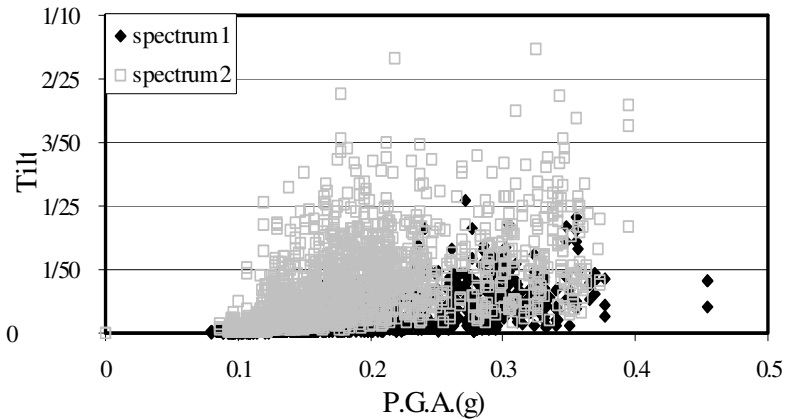


Figure 7. Scatter plots of maximum foundation tilt with respect to peak ground acceleration – Effect of different response spectra

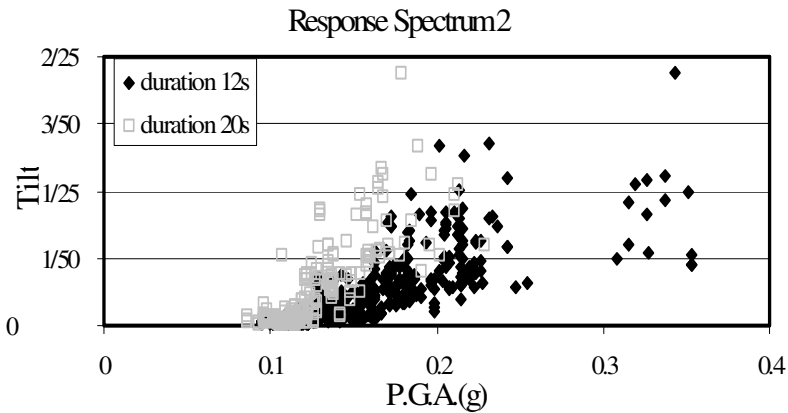


Figure 8. Scatter plots of maximum foundation tilt with respect to peak ground acceleration – Effect of duration of strong ground motion

where $a(t)$ is the ground acceleration and T_d is the effective duration of the earthquake. Figure 9 provides scatter plot of the maximum tilt with respect to I_{Arias} keeping all cases (runs) as in Fig. 7. The Arias intensity provides a somehow better measure of the earthquake intensity because the integral of the square of the acceleration is not divided by the duration (as in I_{rms}). As a result, the bias from the non-converging (interrupted) cases is relatively smaller when using I_{Arias} . It is observed again in Fig. 9 that response spectrum 2 provides higher values for the maximum response than spectrum 1. This demonstrates the inability of I_{Arias} to incorporate information about the frequency content of strong ground motion. Similar conclusions can be drawn for I_{rms} .

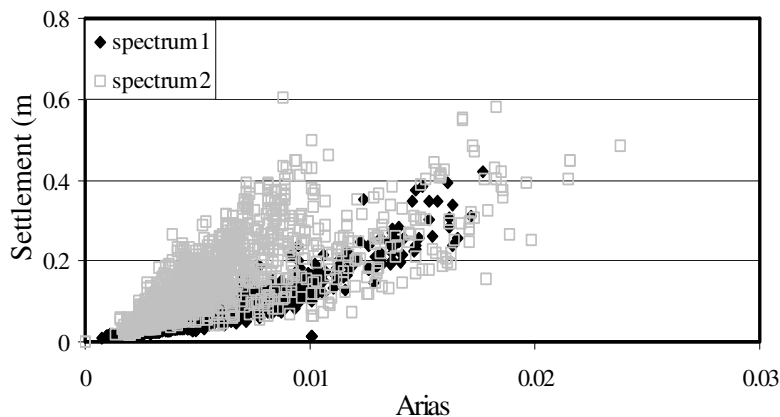


Figure 9. Scatter plots of maximum foundation tilt with respect to Arias intensity – Effect of different response spectra

Fragility curves constitute a useful and concise tool for studying the behavior of a system over a large range of seismic intensities. Specifically, they provide the probability of exceeding a certain damage level as a function of the severity of the seismic event. In this study, since only one footing

was considered, the damage to the superstructure is defined in terms of the maximum tilt. Three levels of damage were identified according to Grant et al. (1974) and Whitman (1979):

The threshold for minor damage was defined for tilt of 1/500, for medium damage for tilt of 1/300 and for major damage for of 1/150. For the construction of fragility curves, it was assumed that for every case where the finite element algorithm diverged, the system sustained major damage.

Figure 10 provides fragility curves, for the problem defined in Fig. 1, with respect to I_{Arias} . Note that different sets of curves are provided for each response spectrum considered. The major usefulness of fragility curves in geotechnical earthquake engineering is clearly demonstrated. First, they provide detailed probabilistic information concerning the behavior of the soil-structure system over a large range of earthquake intensities. This information is provided in terms of exceedance probabilities of three different damage levels and is of paramount importance in estimating damage from a potential earthquake in a prescribed geographical area. The significant differences between the two different sets of fragility curves corresponding to the two response spectra used, indicate that I_{Arias} is not a sufficiently good measure of the severity/intensity of the earthquake in this problem. This comes as no big surprise as it doesn't incorporate any information about the frequency content of the earthquake. The same deficiency is observed when using PGA or I_{rms} .

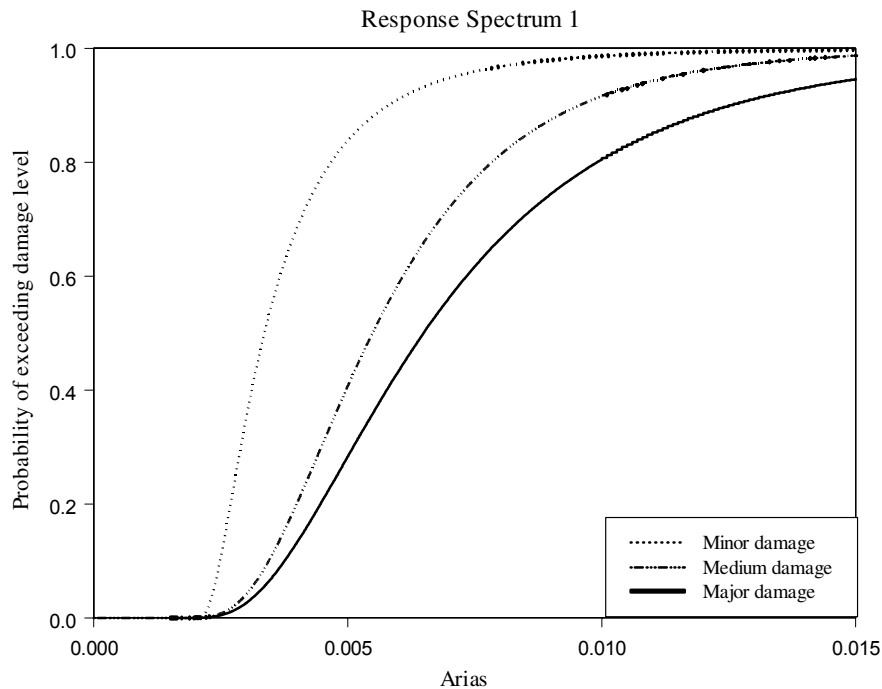


Figure 10. Fragility curves of problem defined in Fig. 1 with respect to Arias intensity for Spectrum 1 – Effect of different response spectra

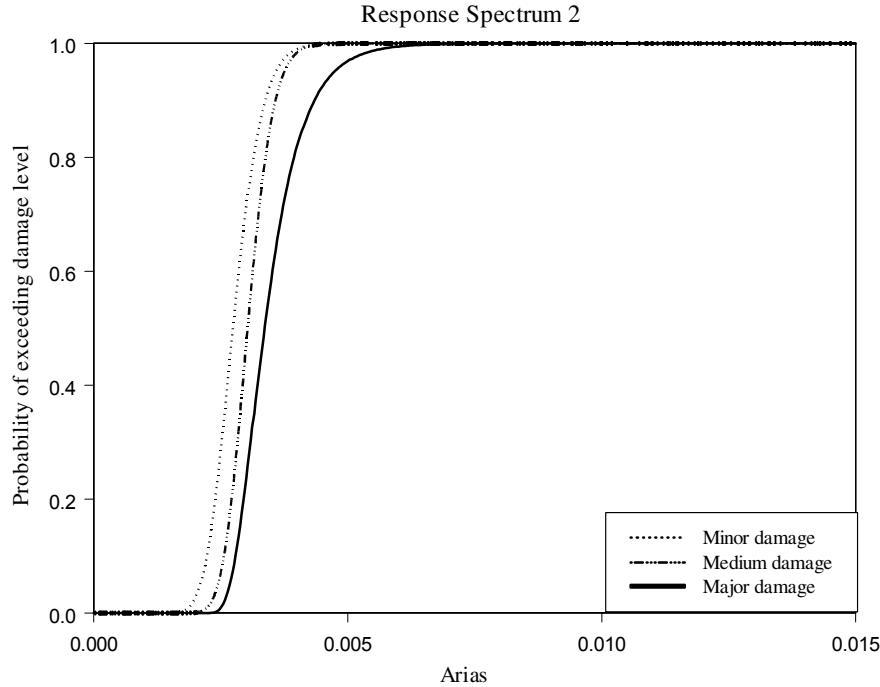


Figure 11. Fragility curves of problem defined in Fig. 1 with respect to Arias intensity for Spectrum 2 – Effect of different response spectra

5.3 Results of Stochastic Analysis - Effect of Natural Frequency of the Structure

In the results presented so far, the data was processed cumulatively and irrespectively of the frequency of the single degree of freedom system that lies on top of the foundation and represents the superstructure. Figure 11 provides fragility curves for three different oscillator frequencies ranging from 3 rad/sec up to 10 rad/sec. These curves are established for medium damage, response spectrum 1, and strong ground motion duration of 12sec. The minor differences among the three curves lead us to the conclusion that the frequency of the oscillator does not have a significant effect on the results. Similar behavior was observed in all other cases of damage level, response spectrum and strong ground motion duration examined.

6 SENSITIVITY ANALYSIS FOR DERIVATIVE SOIL PARAMETERS

It is reminded that the only soil property described a priori as a stochastic field is the cone tip resistance. Once a sample field of CPT values is generated over the domain of the problem, all other soil properties are computed from the simulated CPT values through empirical (deterministic) relations. It is therefore quite interesting to estimate the extent of the relative effect of each one of these derivative soil properties on the response of the system.

In order to reduce the computational cost, the sensitivity analysis focuses on only six parameters P_i , $i = 1, 2, \dots, 6$. Specifically, the permeability \mathbf{k} ($P_1 = \mathbf{k}$), the low strain shear modulus G_0 ($P_2 = G_0$), the low strain bulk modulus B_0 ($P_3 = B_0$), the friction angle φ ($P_4 = \varphi$), the dilation angle φ ($P_5 = \varphi$), and the dilation parameter X_{pp} ($P_6 = X_{pp}$).

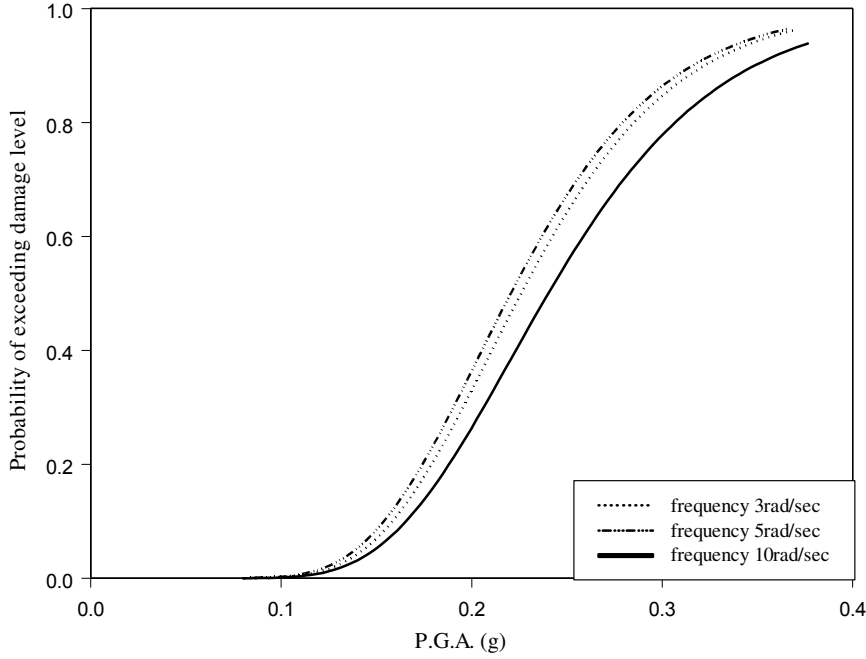


Figure 12. Fragility curves for three different oscillator frequencies (medium damage level, response spectrum 1 and duration 12sec)

The reference values for those parameters, denoted by P_i^0 , are calculated using the average CPT values, $CPT^{av}(z)$. Since there is no dependence on the horizontal coordinate, the properties vary only with depth. The reference values were then fluctuated, one at a time, by 20%: $\Delta P_i = 0.2P_i^0$. The subsequent variability V_i in the response $R(P_1, P_2, P_3, P_4, P_5, P_6)$, because of variability of soil parameter P_i , was measured using the following expression:

$$V_i = \frac{\Delta R_i}{R^0}, i = 1, 2, \dots, 6 \quad (5)$$

where:

$$\Delta R_i = R(P_1^0, P_2^0, \dots, P_i^0 + \frac{1}{2}\Delta P_i, \dots, P_6^0) - R(P_1^0, P_2^0, \dots, P_i^0 - \frac{1}{2}\Delta P_i, \dots, P_6^0)$$

$$R^0 = R(P_1^0, P_2^0, \dots, P_6^0)$$

Only one frequency for the superstructure ($\omega = 5 \text{ rad/sec}$) was considered, since it was found in Section 4 that it has a negligible effect on the response.

6.1 Results and conclusions of sensitivity analysis

Representative results for the variability V_i in the maximum tilt and spectrum 1 are plotted in Fig. 12. The most important conclusion that was drawn was that the friction angle is the parameter that overall has the biggest influence on the response. The shear modulus appears to be dominant for small P.G.As. Its relative effect subsides for higher P.G.As, as it becomes secondary to the friction

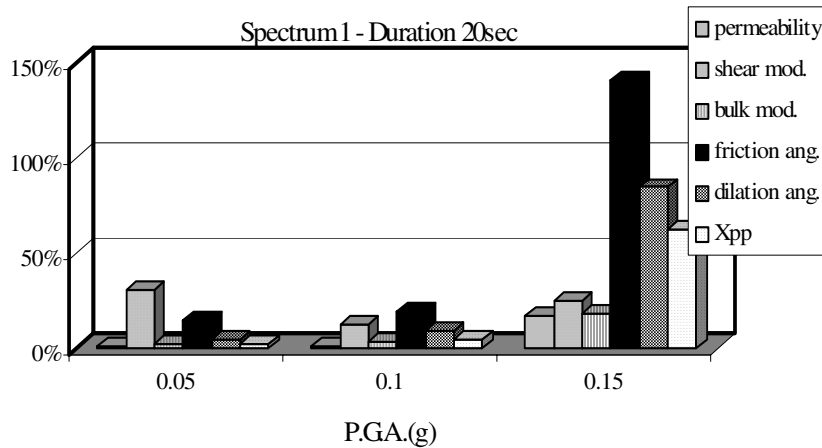


Figure 13. Variability of maximum foundation tilt due to the variability of the six selected soil parameters

and dilation angles. The bulk modulus as well as the dilation parameter seems to play smaller roles. It is rather surprising that the permeability has the smallest effect on the variability of the response, since it is directly related to the development and dissipation of pore water pressures. However, it should be pointed out that the in-situ measurement of the permeability is notoriously difficult. Errors can easily reach or exceed one order of magnitude. The $\pm 10\%$ variability considered here is therefore quite small.

Finally, it was observed that the variability of the response V_i is generally higher for response spectrum 2 compared to response spectrum 1, and for the 20 sec duration compared to the 12 sec duration. This behavior was expected and is observed for every one of the six soil parameters considered.

7 ACKNOWLEDGEMENTS

This work was supported by a grant from the National Science Foundation (NSF Grant # 9523092 with Dr. Clifford Astill as Program Director). Also, computer time was provided by the Princeton Materials Institute, W.M. Keck Computational Materials Center. Both sources of support are most gratefully acknowledged.

8 REFERENCES

- Bendat, J.S. & Piersol, A.G. 1986. *Random Data: Analysis and Measurement Procedures*. John Wiley.
- Benjamin, J. & Cornell A. 1970. *Probability, Statistics and Decision for Civil Engineers*. McGraw-Hill.
- Deodatis, G. 1996. Non-stationary Stochastic Vector Processes: Seismic Ground Motion Applications. *Prob. Eng. Mech.* 11: 149-167.
- Fenton, G.A. 1999, Estimation for stochastic soil models. *Journal of Geotechnical and Geoenvironmental Engineering*. 125(6): 470-485.
- Gasparini, D.A. & Vanmarcke, E.H. 1976. Simulated Earthquake Motions Compatible with Prescribed Response Spectra. *MIT Report No. R76-4*.
- Grant R., Christian J. & Vanmarcke, E.H. 1974. Differential Settlement of Buildings. *Journal of the Geotechnical Engineering Division* GT9: 973-991.

- Griffiths, D.V. & Fenton, G.A. 2000. Influence of soil strength spatial variability on the stability of an undrained clay slope by finite element methods. *Slope Stability 2000*, ASCE Geotechnical Specialty Publication, No.101
- Grigoriu, M. 1995. *Applied Non-Gaussian Processes*. Hemel Hempstead: Prentice Hall.
- Gulf Canada Resources Inc. 1984. Frontier Development - Molikqap, Tarsiut Delineation - 1984/85 Season. *Technical Report 84F012*, Gulf Canada Resources Inc.
- Jefferies, M.G., Rogers, B.T., Stewart, H.R., Shinde, S., James, D. & Williams-Fitzpatrick, S. 1988. Island Construction in the Canadian Beaufort Sea. *Proc. ASCE Spec. Conf. Hydr.*: 816-883.
- Jefferies, M.G., Stewart, H.R., Thompson, R.A.A. & Rogers, B.T. 1985. Molikqap Development at Tarsiut P-45. *Proc. Conf. Arctic '85*: 1-27.
- Jennings, P.C., Housner, G.W. and Tsai, N.C. (1968). Simulated Earthquake Motions. *Technical Report, Earthquake Engineering Research Laboratory*, California Institute of Technology.
- Mathies, H. & Strang, G. 1979. The Solution of Nonlinear Finite Element Equations. *Int. Jnl. Num. Meth. Eng.* 14: 1613-1626.
- Popescu, R. 1995. Stochastic Variability of Soil Properties: Data Analysis, Digital Simulation, Effects on System Behavior. Dissertation, Princeton University.
- Popescu, R., J.H. Prévost, J.H. & Deodatis G. 1997. Effects of Spatial Variability on Soil Liquefaction: Some Design Recommendations. *Geotechnique*. 47(5): 1019-1036.
- Popescu, R., Deodatis, G. & Prévost, J.H. 1998. Simulation of Homogeneous Non-Gaussian Stochastic Vector Fields. *Probabilistic Engng. Mech.* 13(1): 1-13.
- Prévost, J.H. 1980. Mechanics of Continuous Porous Media. *Int. J. Eng. Science*. 18(5): 787-800.
- Prévost, J.H. 1985. A Simple Plasticity Theory for Cohesionless Frictional Soils. *Int. J. Soil Dyn. Earthq. Eng.*, 4(1): 9-17.
- Prévost, J.H. 1999. DYNAFLOW - A Nonlinear Transient Finite Element Analysis Program - User Manual. Princeton University.
- Prévost, J.H. & Keane, C.M. 1990. Shear Stress-Strain Curve Generation from Simple Material Parameters. *J. Geotech. Eng. ASCE* 116(GT8): 1255-1263.
- Shinozuka, M. & Deodatis, G. 1991. Simulation of Stochastic Processes by Spectral Representation. *Appl. Mech. Rev.* ASME 44: 191-204.
- Shinozuka, M. & Deodatis G. 1996. Simulation of multi-dimensional Gaussian Stochastic Fields by Spectral Representation. *Appl. Mech. Rev.* ASME 49: 29-53.
- Whitman, R. 1979. *Soil Mechanics*. New York:Wiley.